This article has been accepted for publication in a future issue of this journal, but has not been fully edited. Content may change prior to final publication. Citation information: DOI 10.1109/JSEN.2019.2945002, IEEE Sensors Journal

Isotope shift of nuclear magnetic resonances in ^{129}Xe and ^{131}Xe caused by spin-exchange pumping by alkali metal atoms

Vladimir I. Petrov, Anatoly S. Pazgalev, and Anton K. Vershovskii

sds

***Abstract*—The effect of isotope shifts of nuclear magnetic resonance (NMR) frequency in xenon isotopes ^{129}Xe and ^{131}Xe polarized by optically-oriented alkali metal atoms is not only of fundamental interest, but also of practical significance, since it is the main factor limiting the accuracy of a whole class of prospective navigation and metrological devices. Our study of the parametric dependences of the isotope shift has shown that this effect is largely due to incomplete averaging of an inhomogeneous local magnetic field by two xenon isotopes, and therefore, its value can be influenced by applying an external magnetic field gradient. A numerical model is derived that qualitatively describes the effect of the isotopic frequency shift, as well as its dependence on the cell temperature and the external magnetic field gradient. The model provides a good quantitative agreement with the experiment – e.g., at a temperature of 85°C, the isotope shift values predicted by the model coincide with experimental data with an accuracy of up to the experimental error, which, in turn, does not exceed 8% of the total change in the isotopic shift in the entire range of applied magnetic field gradients.**

***Index Terms*—Nuclear magnetic resonance, xenon isotopes, optical pumping, spin-exchange pumping**

I. Introduction

ATOMIC NUCLEI for which direct optical pumping is not feasible can be polarized in the process of interaction with oriented alkali metal atoms (i.e., K, Rb, Cs, hereinafter referred to as Me) [1]. This process, known as spin-exchange pumping, is particularly efficient for xenon due to the formation of weakly-coupled van der Waals molecules Me-Xe [2,3,4]. An additional two- or three-order amplification of the NMR signal in Xe is achieved due to the Fermi-contact hyperfine interaction with Me atoms [5].

Polarized xenon nuclei have found applications in medicine [6,7], navigation [8–10], precision measurement of the magnetic field [11], and search for fundamental interactions that do not preserve the local symmetry [12,13].

In [12], the magnetic resonance signal of odd xenon isotopes was used to search for long-range interactions involving axions and axion-like particles. The authors observed an effect which they called an isotope shift (IS). This effect shows itself in a mismatch of the values of the magnetic field measured by the ^{129}Xe and ^{131}Xe isotopes in a volume common to oriented rubidium atoms. Under these conditions, optically-oriented alkaline atoms create a local magnetic field in the cell volume. Contact interaction leads to an effective k_{XeMe}-fold increase in the magnetic field created by Xe nuclei and detected by Me atoms and to a $k_{MeXe} \approx k_{XeMe}$-fold increase of the field created by Me atoms and detected by Xe nuclei. In the subsequent discussion, we shall use the term "an *effective* field" to refer to the magnetic field strengthened by the contact interaction. The effective field created by oriented Me atoms in the cell will be called an internal field B_a.

In [5], there is no indication that the coefficients k_{MeXe} may be different for the two xenon isotopes. Nevertheless, in the experiment [12], it was observed that the ratio of frequencies of NMR in xenon isotopes changed with the internal field B_a. The corresponding difference between the effective fields measured by the two ΔB isotopes was called an isotope shift. Quantitatively, the shift magnitude is described by the dimensionless quantity δB_A expressed through the ratio of the precession frequencies f_i (i = 1, 2 for ^{129}Xe and ^{131}Xe):

$$\frac{f_1}{f_2} = \rho \cdot \left(1 + \frac{\Delta B}{B_0}\right) = \rho \cdot \left(1 + \delta B_A \cdot \frac{P \cdot B_A}{B_0}\right), \quad (1)$$

where $\rho = |\gamma_1/\gamma_2|$, γ_i (i = 1,2) are the gyromagnetic ratios of isotopes; P is the degree of polarization of the alkali metal atoms; B_A is the effective field that the metal atoms would create in the case of complete (P = 1) polarization; then the internal field is $B_a = P \cdot B_A$, and $\Delta B = \delta B_A \cdot B_a$.

The questions of the IS nature as well as of its dependence on the parameters of the experiment remain open. However, these questions are both of fundamental and applied significance, since IS leads to the emergence of ΔB dependence on the internal field. Therefore, it has a decisive destructive effect on the accuracy of the whole class of prospective navigation devices using xenon NMR [9–11,14,15].

Furthermore, being the most accurate instruments in their class, quantum metrological sensors are used to search for physical interactions that go beyond the Standard Model. Correct estimation of the systematic error of these devices determines the upper bound of the parameter domain of

V. I. Petrov is with the Concern CSRI Elektropribor, JSC, 197046, St. Petersburg, Russia, 30 Malaya Posadskaya str. (e-mail: icins@eprib.ru).

A. S. Pazgalev is with the Ioffe Institute, 194021, St. Petersburg, Russia, 26 Politekhnicheskaya (e-mail: anatoly.pazgalev@mail.ioffe.ru).

A. K. Vershovskii is with the Ioffe Institute, 194021, St. Petersburg, Russia, 26 Politekhnicheskaya (e-mail: antver@mail.ioffe.ru).

1558-1748 (c) 2019 IEEE. Personal use is permitted, but republication/redistribution requires IEEE permission. See http://www.ieee.org/publications_standards/publications/rights/index.html for more information.

This article has been accepted for publication in a future issue of this journal, but has not been fully edited. Content may change prior to final publication. Citation information: DOI 10.1109/JSEN.2019.2945002, IEEE Sensors Journal

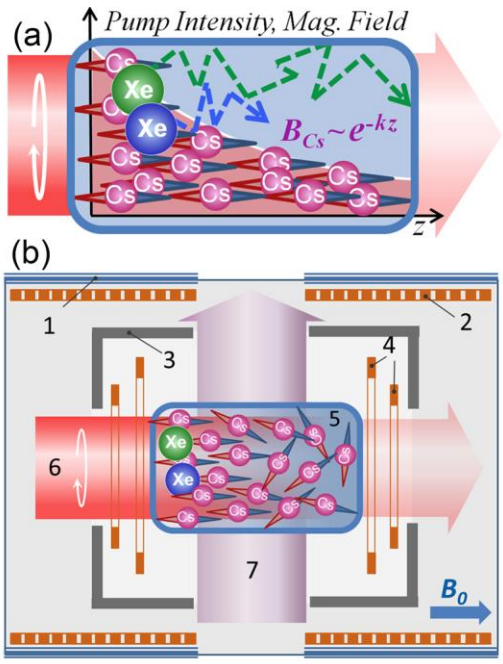

Fig. 1. a) The explanation for the isotope shift: the spatial distribution of the pumping light intensity, the Cs (or Rb) polarization, and the internal magnetic field in the cell. b) Simplified experimental setup: 1 – multi-layer magnetic shield, 2 – solenoid, 3 – thermostat, 4 – anti-Hemholtz magnetic coils, 5 – cell, 6 – pumping beam, 7 – probe beam.

hypothetical interactions, and is the subject of an extensive study. Thus, reference [16] considered the factors determining the accuracy of the ^{129}Xe-^{3}He-magnetometer. The precession frequencies of xenon and helium were compared in the absence of an effective field B_a. It was shown that the ratio of NMR frequencies is affected by the quadratic field gradient as well as the temperature gradient in the cell, which was explained by the fact that the temperature gradient causes a concentration gradient that turns out to be different for two atomic ensembles with mismatched diffusion constants. However, the estimates show that the IS effect reported in [12] cannot be explained in this way, since the difference between the diffusion constants of two xenon isotopes is obviously too small, as is the temperature gradient in the compact cell used in [12].

In [15], we proposed the following explanation for the IS effect (Fig.1a):

- absorption of the pumping light along the z-direction by Me atoms leads to a non-uniform spatial distribution of pumping intensity $I_P(z)$ over the cell;
- polarization of Me atoms $P(z)$ is distributed according to the same law, since the diffusion of Me can be neglected due to the short length of the diffusion path of oriented atoms as compared with the length of the cell;
- spin-exchange pumping of Xe isotopes takes place predominantly in the region of the highest alkaline metal polarization, that is, in the frontal area of the cell;
- the internal field $B_a(z)$ follows the distribution of $P(z)$, which gives rise to the gradient $dB_a(z)/dz$.

Thus, in the region where xenon nuclei are oriented with maximum probability, they experience the effect of the local internal field that exceeds the average internal field. Diffusion of xenon atoms throughout the cell leads to an effective averaging of the spatially inhomogeneous field measured by atoms. The longer is the isotope relaxation time, the closer is the value of the field measured by it to the average across the cell.

The difference in the transverse relaxation times T_i of the two Xe isotopes results in different mean fields, that is, emergence of an IS. In [15], we measured the IS dependence on temperature and showed that the IS effect vanishes at a temperature that provides an approximate equality of T_i. The effect of the internal gradient on xenon T_i was previously described in [16] and it was later studied in [17]. In these publications, it was proposed to reduce the ^{129}Xe relaxation, compensating for the internal field gradient using an external gradient; but the question of the effect produced by the field and its gradients on IS was not raised.

In this paper, we built a numerical model that allows us to calculate the magnitude of IS, and obtained a new expanded set of experimental data, which allowed us to test the model and thereby confirm our explanation of the nature of IS.

II. Experimental

The experiment (Fig.1b) was carried out on a setup described in [15]. The setup was assembled in accordance with a two-beam scheme [18] with pumping by a circularly-polarized beam, resonant to the D_1 line of ^{133}Cs and directed along the vector of the constant magnetic field B_0 (axis z). The EPR signal in cesium was detected by recording the rotation of the polarization plane of the transverse (i.e., directed along the x-axis) linearly-polarized beam detuned from the D_1 line of Cs. The 5 mm cubic cell contained Cs vapor, 20 Torr N_2, and 30 Torr natural Xe (which, in turn, contains 26.4% of ^{129}Xe, 21.2% of ^{131}Xe, and zero-spin isotopes, acting as a buffer gas).

The magnetic field B_0 was stabilized at a level of 12 μT; the field's instability over the measurement time did not exceed a few unities of pT. The setup included a set of coils to create a linear magnetic field gradient along the pumping axis. Unlike in [15], the set of coils was complemented with two compensating windings, which made it possible to eliminate errors shifts by its effect on the sensor of the magnetic field stabilizer.

Optical pumping of cesium was alternately performed by the light of the left and right circular polarization; the pumping light intensity was ~ 10 mW. The central part of the wide Gaussian beam was used to provide a compromise between power losses (about 30%) and beam inhomogeneity. The precession of Xe nuclear moments was initiated with a π/2 pulse of a transverse resonant RF field. Switching of the pumping light polarization resulted in a change in the direction of the internal field vector, and thus, led to shifts in the isotope i = 1,2 precession frequencies:

$$f_i^{\pm} = \frac{\gamma_i}{2\pi}\left(B_0 \pm \left(1-(-1)^i \cdot \frac{\delta B_A}{2} \pm \frac{\kappa}{2}\right)\cdot B_a \right), \qquad (2)$$

1558-1748 (c) 2019 IEEE. Personal use is permitted, but republication/redistribution requires IEEE permission. See http://www.ieee.org/publications_standards/publications/rights/index.html for more information.

This article has been accepted for publication in a future issue of this journal, but has not been fully edited. Content may change prior to final publication. Citation information: DOI 10.1109/JSEN.2019.2945002, IEEE Sensors Journal

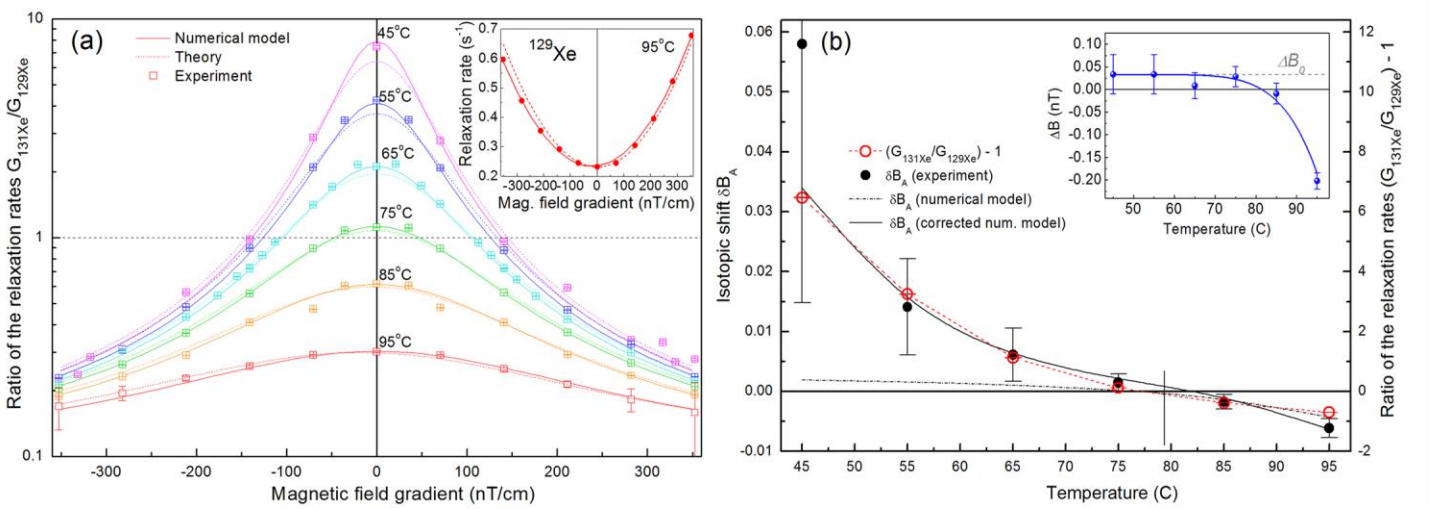

Fig. 2. a) Dependence of the ratio of the relaxation rates of isotopes on the gradient of the external magnetic field at different temperatures. Inset: dependence of the relaxation rate of ^{129}Xe on the field gradient at 95°C. Dotted lines: calculation of the G_{129Xe} dependence on the field gradient according to[19]. Solid lines: the numerical simulation results. b) Temperature dependence of δB_A at zero external field gradient. Black circles: experiment. Dash-dotted line: numerical calculation. Solid line: the numerical simulation results taking into account low-temperature factors. Red hollow circles and red short-dotted line: the ratio of the relaxation rates of isotopes (G_{131}/G_{129}) – 1. Inset: temperature dependence of the difference ΔB of the fields measured by Xe isotopes at zero external field gradient.

where f_i^- and f_i^+ are the precession frequencies measured at two pumping polarizations, and $\kappa \cdot B_a$ is a small ($\kappa << 1$) change in the effective field B_a caused by the imperfection of the circular polarizer.

According to (1), based on the results of four frequency measurements, we can obtain δB_A, B_a, $\rho = \gamma_1/\gamma_2$ and $\kappa \cdot B_a$:

$$B_a = \frac{2B_0}{\left(\frac{1}{\delta f_1 + \delta f_2}\right) - \left(\frac{\kappa}{4}\right)} \approx 2B_0\left(\delta f_1 + \delta f_2\right), \quad (3)$$

$$\delta B_A = 2\frac{\delta f_1 - \delta f_2}{\delta f_1 + \delta f_2}, \quad (4)$$

where $\delta f_i = (f_i^+ - f_i^-)/(f_i^+ + f_i^-)$. From (3) and (4) it follows that κ makes only a small contribution to the value of B_a and does not make any contribution to the value of δB_A. The values of δB_A, B_a, T_i were measured as a function of temperature in the range of 45–95°C (which corresponds approximately to a 50-fold change in the alkali density) and the gradient of the external magnetic field in the range of dB_z/dz = -350...+350 nT/cm. The internal magnetic field value B_a was measured to be ~ 16 nT at T = 85°C; this value scaled with the Cs vapor density.

The transverse relaxation rates $G_i = 1/T_i$ obtained in the experiments were compared with the theory predictions [3,4] (Fig.2a) and with the results of our numerical simulation.

As follows from Fig. 2b, IS becomes zero at a temperature that provides an approximate equality of the isotope relaxation rates: T_0 = 79.5°C. The inset in Fig. 2b shows that a rapid increase in δB_A in the low-temperature region corresponds to a constant difference in the ΔB values of the fields measured by two isotopes: ΔB = (33 ± 10) pT. This fact cannot be explained in the framework of our model; it will be discussed below.

III. Numerical Simulation

We developed a simple one-dimensional model of the system, allowing for calculation of the temperature dependences of δB_A and G_i and the external gradient dB_z/dz (Fig. 2–4). The cell with the size L along the z-axis was divided by J = 16..64 layers (layer's thickness $\Delta z = L/J$). The distribution of all system parameters inside each layer was considered uniform. The pumping intensity $I_p(j)$ and the number of oriented cesium atoms $Ncs_j = Ncs(j)$ in each layer $j = 1..J$ were calculated taking into account the nonlinearity of absorption in the optically dense medium. The relaxation of Cs atoms on the cell walls was modeled as the function $f_{rel}(j) = (j/(j+\lambda_{Cs}/\Delta z))\cdot((J-j)/(J-j+\lambda_{Cs}/\Delta z))$, where λ_{Cs} is the diffusion length of oriented cesium. The simulation time step Δt was taken equal to the diffusion time of Xe through a layer of thickness Δz: $\Delta t = \Delta z^2/D$, where D is the coefficient of Xe diffusion.

The distribution of polarized xenon nuclei $Nxe_{ij} = Nxe_i(j)$ was described by an array of complex numbers $|Nxe_{ij}|\cdot exp(i\varphi_{ij})$, where φ_{ij} is the instantaneous precession phase of Xe_i isotope in layer j. The phase evolution of one "generation" of a polarized nuclei ensemble was estimated numerically. It was assumed that the distribution of $Nxe_i(j)$ at the initial time t = 0 follows the normalized distribution of $Ncs(j)$, and at subsequent points in time $(t = (n-1)\cdot\Delta t)$ evolves under the effect of diffusion, relaxation, external and internal magnetic fields, and their gradients.

The process of establishing the stationary distribution of Nxe_1 is shown in Fig.3a. The evolution of the array Nxe_i at the calculation step n is described by equation (5):

1558-1748 (c) 2019 IEEE. Personal use is permitted, but republication/redistribution requires IEEE permission. See http://www.ieee.org/publications_standards/publications/rights/index.html for more information.

This article has been accepted for publication in a future issue of this journal, but has not been fully edited. Content may change prior to final publication. Citation information: DOI 10.1109/JSEN.2019.2945002, IEEE Sensors Journal

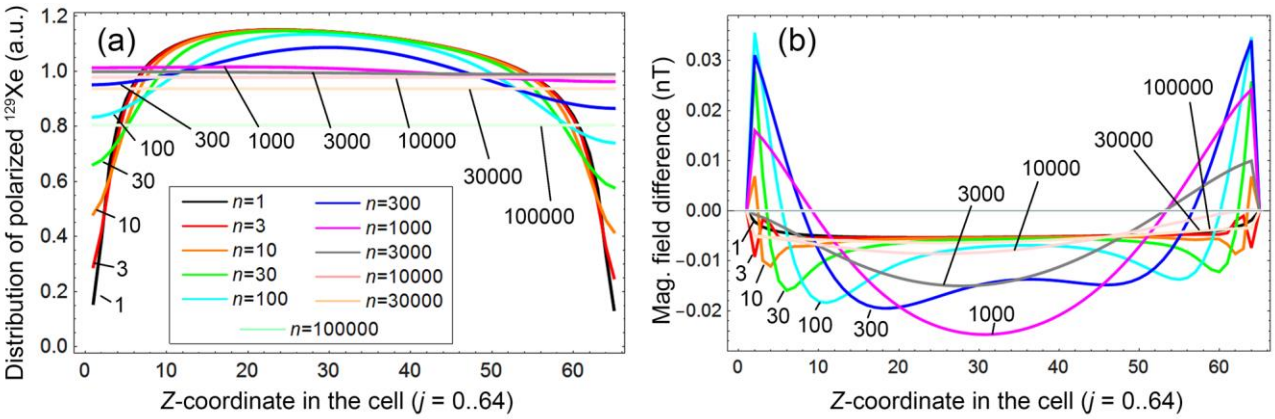

Fig. 3. Results of the numerical simulation at T = 85°C: a) spatial distribution of oriented ^{129}Xe atoms in the cell at times $t = (n-1)\cdot\Delta t$, where n = 1, 3, 10, 30.., Δt = 55 μs; the n = 1 curve also describes the distribution $Ncs(z)$ of oriented Cs, and the distribution of the internal field $B_a(z)$; b) the difference of the magnetic fields [nT] measured by ^{129}Xe and ^{131}Xe isotopes in the cell under the same conditions

$$Nxe_{i,n} = \left(1 - \frac{\Delta t}{\vartheta_{i,j}\cdot T_i}\right)\cdot \begin{bmatrix} (1-k_i)\cdot e^{i\gamma_i B_1 \Delta t} & k_i\cdot e^{i\gamma_i B_1 \Delta t} & 0 & \dots & 0 \\ k_i\cdot e^{i\gamma_i B_2 \Delta t} & (1-2k_i)\cdot e^{i\gamma_i B_2 \Delta t} & k_i\cdot e^{i\gamma_i B_2 \Delta t} & \dots & 0 \\ 0 & k_i\cdot e^{i\gamma_i B_3 \Delta t} & (1-2k_i)\cdot e^{i\gamma_i B_3 \Delta t} & \dots & 0 \\ \dots & \dots & \dots & \dots & \dots \\ 0 & 0 & 0 & \dots & (1-k_i)\cdot e^{i\gamma_i B_N \Delta t} \end{bmatrix} \cdot Nxe_{i,n-1}, \quad (5)$$

where B_1, B_2, etc. denote the magnetic field in each layer, $k_i \approx 1/4$ are the probabilities of transition from layer j to layer $j\pm1$ for the Xe_i isotope, and $\vartheta_{i,j}$ are coefficients describing relaxation on the cell walls.

The three-diagonal structure of the evolution operator matrix reflects the fact that during the period of Δt, the diffusion process only binds the nearest adjacent layers. According to kinetic theory, the coefficients of isotope diffusion differ in accordance with the ratio of the roots of their masses; for xenon, $D_1/D_2 \approx 1.0077$. This difference was taken into account in the model; however, it showed up only at the initial steps of the system evolution (the peaks on Fig.3b), and did not lead to any noticeable integral results.

The values of the local magnetic field B_j are the sum of the values of the local internal field B_{aj} and the local field due to the external magnetic field gradient applied to the cell. In expression (5), we do not take into account the precession caused by the field B_0, since it is the same in all layers of the cell and at all instants of time. In other words, we measure the precession phase of each isotope Xe_i in a coordinate system rotating with a frequency $\gamma_i \cdot B_0$.

To speed up the calculations, we restricted the description of exponential decay to the first member of the Taylor series. In order to account for the fact that the relaxation of ^{131}Xe occurs on the cell surface as well as in the volume [1,2], we assumed that the ^{131}Xe relaxation rate is higher in $j = 1$ and $j = J$ layers (and correspondingly lower in all other layers) than the mean relaxation rate G_2. Therefore, in equation (5) we used $\vartheta_{1,j} = 1$, $\vartheta_{2,1} = \vartheta_{2,J} < 1$, and $\vartheta_{2,j} > 1$ for $1 < j < J$.

Next, we monitored the evolution of the system during the $3T_1$ period (or $3T_2$, whichever is the greater). At each step n, the measurement of the xenon precession phases $\varphi_{i,j,n}$ by cesium was simulated. For this, the phases $\varphi_{i,j,n}$ were averaged over the cell with weights determined by the cesium distribution Ncs – this way we took into account the fact that the contribution of each layer to the mean phase measured by Cs atoms is proportional to the number of Cs atoms in this layer.

Based on the rate of change of the precession phase, we calculated the mean magnetic fields measured by the Xe isotopes at each step:

$$B_{i,n} = \frac{\varphi_{i,n} - \varphi_{i,n-1}}{\Delta t \cdot \gamma_i}, \quad (6)$$

and then averaged these fields over all evolution time:

$$B_i = \frac{\sum_n \left(\sum_j \left| Nxe_{i,j,n} \right| \cdot B_{i,n} \right)}{\sum_{j,n} \left| Nxe_{i,j,n} \right|}. \quad (7)$$

Then we calculated B_a and δB_a according to (1):

$$B_a = (B_1 + B_2)/2, \quad (8)$$

$$\delta B_a \approx (B_1 - B_2)/B_a. \quad (9)$$

1558-1748 (c) 2019 IEEE. Personal use is permitted, but republication/redistribution requires IEEE permission. See http://www.ieee.org/publications_standards/publications/rights/index.html for more information.

This article has been accepted for publication in a future issue of this journal, but has not been fully edited. Content may change prior to final publication. Citation information: DOI 10.1109/JSEN.2019.2945002, IEEE Sensors Journal

The rate of change of the absolute value $|Nxe_{i,n}|$ was used to calculate the real (determined by the magnetic field gradient) relaxation times T_i and relaxation rates G_i:

$$G_i = \frac{-\ln\left(\sum_j \left|Nxe_{i,j,n}\right| / \sum_j \left|Nxe_{i,j,1}\right|\right)}{(n-1)\cdot\Delta t}. \quad (10)$$

The dependences of T_i on the field gradient is consistent with the theoretical predictions, with the accuracy of the coefficient close to unity [19]. The inset in Fig.2a shows that the dependence of the ^{129}Xe relaxation rate has a minimum for a nonzero external gradient, which is due to the influence of the internal field linear gradient discovered earlier [14,16,17]. The numerical simulation adequately describes the experimentally measured horizontal shift of this dependence.

The analysis of the simulation results (Fig. 3,4) has shown that the inhomogeneity of alkali metal polarization, caused by the relaxation of the alkali metal on the cell walls, plays a significant role in IS; therefore, to describe IS more accurately, it is necessary to take into account the near-wall relaxation during Cs diffusion in all directions, i.e., to build a three-dimensional numerical model.

The experiment revealed a difference in the Xe_i precession frequencies corresponding to a constant difference in the ΔB values of the fields measured by two isotopes that is not described by the proposed model. The discrepancy is especially noticeable at low temperatures $T \leq 65^{o}$C, at which the value of the internal field is small. In this case, the difference in the ΔB values of the fields measured by two isotopes is caused by a change in the sign of the circular polarization itself rather than by the internal field, and it was found to be $\Delta B = (33 \pm 10)$ pT (inset in Fig.2b).

This effect may be explained by the asymmetry of the composite line of the ^{131}Xe magnetic resonance. In a cell that has an asymmetric shape, the ^{131}Xe line is split into three components [20,21]. When the amplitudes of the components are unequal, a change in the polarization sign can lead to a shift similar to the orientation shift in frequency of the cesium magnetometer. The estimates show that a 2–3 percent difference in the cell size is sufficient to explain the effect; the same is true for the order of the asymmetry in the amplitudes of the components of the ^{131}Xe quadrupole structure. An additional source of shifts may be the ^{129}Xe-^{131}Xe coupling, although its value should be small compared to the value of the electron-nuclear Xe-Me interaction.

The correction for the polarization-dependent shift of the ^{131}Xe-magnetometer readings in the model eliminates the discrepancy with the experiment at low temperatures and has little or no effect on the results obtained at temperatures of 75°C and higher.

Fig.4 compares the results of numerical simulation with experimental data; for clarity, Fig.4a shows the results of the 2D experimental data approximation over the whole data array instead of the experimental points. In order to give an idea of the accuracy of the experimental data, Fig. 4a also shows the typical values of experimental errors in vertical bars (the error bars also can be seen in Fig.2b and Fig.4b). As follows from Fig.4b, the model adequately describes the experimental data in the temperature range 55–85°C, with the best fit being achieved at T = 85°C (Fig.4b).

Obviously, at high (> 85°C) temperatures, and, consequently, a high alkali metal concentrations and their gradients, the one-dimensional approximation turns out to be insufficient.

As follows from Fig.4a, the IS effect at any temperature can be nulled by introducing the external magnetic field gradient. Alternatively, it is possible to minimize the dependence of IS on temperature.

Up to this point, we did not discuss the dependence of IS on cell size. The cell size reduction involves a procedure for optimizing the temperature and the gas pressure. Our estimations show that the increase in IS due to acceleration of the wall relaxation of Me and ^{131}Xe can be compensated in the first order by increasing the pressure of the gas mixture. However, the real dependences of the system parameters (primarily, the relaxation rate of ^{131}Xe) on these factors in compact cells have not been adequately explored, and require additional experimental study.

IV. Conclusions

We have studied the dependences of the isotopic shift (IS) and related parameters on temperature and the magnetic field gradient. A simple one-dimensional model has been developed, which describes the evolution of nuclear spins under the conditions of spin-exchange pumping with alkali metal atoms.

It has been shown that in the temperature range of 55–85°C, which is of particular interest for compact NMR sensors, the model shows good agreement with the experiment, which confirms the validity of the explanation for the IS proposed earlier. The model provides the best agreement with the experiment at a temperature of 85°C: the model predicted isotope shift values coincide with the experimental data up to the experimental error, which, in turn, does not exceed 8% of the total change in the isotopic shift in the entire range of applied magnetic gradients. The discrepancies at low temperatures are primarily due to the experimental errors which are growing rapidly with fall of temperature. At higher temperatures, the discrepancy grows due to high density of cesium (the cell becomes optically thick), the non-linear gradients caused by this, and the inability of the one-dimensional model to describe this distribution adequately.

1558-1748 (c) 2019 IEEE. Personal use is permitted, but republication/redistribution requires IEEE permission. See http://www.ieee.org/publications_standards/publications/rights/index.html for more information.

This article has been accepted for publication in a future issue of this journal, but has not been fully edited. Content may change prior to final publication. Citation information: DOI 10.1109/JSEN.2019.2945002, IEEE Sensors Journal

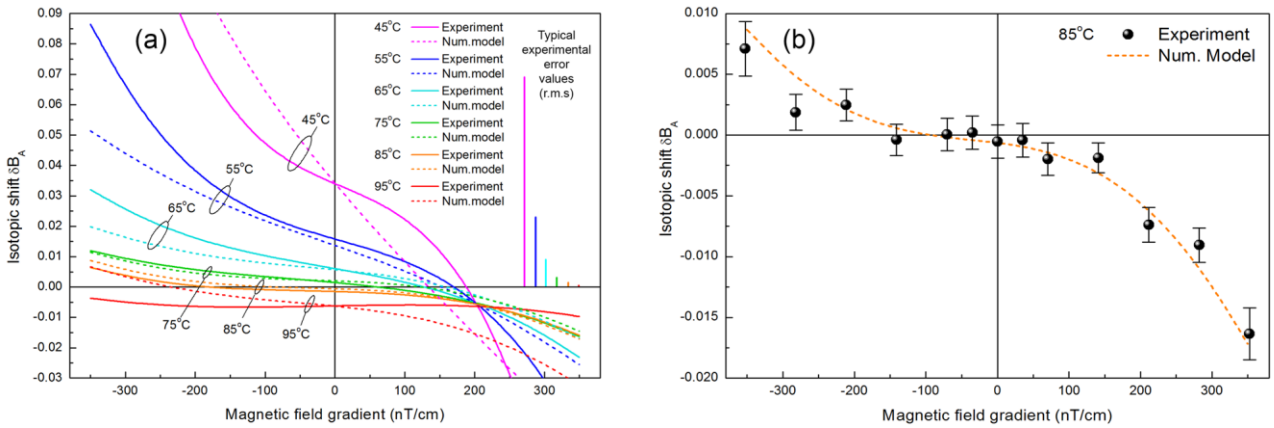

Fig. 4. Comparison of the numerical model with the experiment: (a) Isotopic shift dependence on the external field gradient in wide temperature range; dotted lines: approximation of experimental data; solid lines: numerical simulation, vertical bars: typical experimental error values (r.m.s.). (b) Isotopic shift dependence on the external field gradient at T = 85°C.

In addition, an anomalous IS was observed at low temperatures, and an explanation for it has been proposed.

It has been shown that the isotope shift can be eliminated to a large extent by equalizing the relaxation times of isotopes through an appropriate choice of the optimum temperature and/or compensation for the internal field gradient with the gradient of the external magnetic field.

REFERENCES

[1] M. A. Bouchiat, T. R. Carver, and C. M. Varnum, "Nuclear Polarization in He^3 Gas Induced by Optical Pumping and Dipolar Exchange", *Phys. Rev. Lett.*, vol. 5, no. 8, pp. 373–375, 1960.

[2] C. H. Volk, T. M. Kwon, and J. G. Mark, "Measurement of the ^{87}Rb-^{129}Xe spin-exchange cross section", *Phys. Rev. A*, vol. 21, no. 5, pp. 1549–1555, 1980.

[3] X. Zeng, Z. Wu, T. Call, E. Miron, D. Schreiber, and W. Happer, "Experimental determination of the rate constants for spin exchange between optically pumped K, Rb, and Cs atoms and ^{129}Xe nuclei in alkali-metal–noble-gas van der Waals molecules", *Phys. Rev. A*, vol. 31, no. 1, pp. 260–278, 1985.

[4] T. G. Walker and W. Happer, "Spin-exchange optical pumping of noble-gas nuclei", *Rev. Mod. Phys.*, vol. 69, no. 2, pp. 629–642, 1997.

[5] B. C. Grover, "Noble-Gas NMR Detection through Noble-Gas-Rubidium Hyperfine Contact Interaction", *Phys. Rev. Lett.*, vol. 40, no. 6, pp. 391–392, 1978.

[6] R. S. Virgincar *et al.*, "Quantitative analysis of hyperpolarized 129Xe ventilation imaging in healthy volunteers and subjects with chronic obstructive pulmonary disease", *NMR in Biomedicine*, vol. 26, no. 4, pp. 424–435, 2013.

[7] Y. V. Chang, J. D. Quirk, I. C. Ruset, J. J. Atkinson, F. W. Hersman, and J. C. Woods, "Quantification of human lung structure and physiology using hyperpolarized 129Xe", *Magnetic Resonance in Medicine*, vol. 71, no. 1, pp. 339–344, 2014.

[8] E. Kanegsberg, "A Nuclear Magnetic Resonance (NMR) Gyro With Optical Magnetometer Detection", in *SPIE*, San Diego, United States, 1978, vol. 0157, pp. 73–80.

[9] T. Walker and M. Larsen, "Chapter eight–spin-exchange-pumped NMR gyros", *Adv. At. Mol. Opt. Phys.*, vol. 65, pp. 373–401, 2016.

[10] A. K. Vershovskii, Yu. A. Litmanovich, A. S. Pazgalev, and V. G. Peshekhonov, "Nuclear Magnetic Resonance Gyro: Ultimate Parameters", *Gyroscopy and Navigation*, vol. 9, no. 3, pp. 162–176, 2018.

[11] C. Gemmel *et al.*, "Ultra-sensitive magnetometry based on free precession of nuclear spins", *The European Physical Journal D*, vol. 57, no. 3, pp. 303–320, 2010.

[12] M. Bulatowicz *et al.*, "Laboratory Search for a Long-Range T-Odd, P-Odd Interaction from Axionlike Particles Using Dual-Species Nuclear Magnetic Resonance with Polarized Xe 129 and Xe 131 Gas", *Physical review letters*, vol. 111, no. 10, p. 102001, 2013.

[13] F. Allmendinger *et al.*, "New Limit on Lorentz-Invariance- and CPT-Violating Neutron Spin Interactions Using a Free-Spin-Precession ^{3}He-^{129}Xe Comagnetometer", *Phys. Rev. Lett.*, vol. 112, no. 11, p. 110801, 2014.

[14] Defense Technical Information Center, *DTIC ADA101010: Nuclear Moment Alignment, Relaxation and Detection Mechanisms*. 1981.

[15] A. K. Vershovskii, A. S. Pazgalev, and V. I. Petrov, "The Nature of the Effect of Precession-Frequency Mismatch between 129Xe and 131Xe Nuclei under Spin-Exchange Pumping by Alkali-Metal Atoms", *Technical Physics Letters*, vol. 44, no. 4, pp. 313–315, 2018.

[16] D. Sheng, A. Kabcenell, and M. V. Romalis, "New Classes of Systematic Effects in Gas Spin Comagnetometers", *Phys. Rev. Lett.*, vol. 113, no. 16, p. 163002, Oct. 2014.

[17] X. Liu, C. Chen, T. Qu, K. Yang, and H. Luo, "Transverse spin relaxation and diffusion-constant measurements of spin-polarized 129Xe nuclei in the presence of a magnetic field gradient", *Scientific Reports*, vol. 6, p. 24122, Apr. 2016.

[18] W. E. Bell and A. L. Bloom, "Optical Detection of Magnetic Resonance in Alkali Metal Vapor", *Phys. Rev.*, vol. 107, no. 6, pp. 1559–1565, 1957.

[19] G. D. Cates, S. R. Schaefer, and W. Happer, "Relaxation of spins due to field inhomogeneities in gaseous samples at low magnetic fields and low pressures", *Phys. Rev. A*, vol. 37, no. 8, pp. 2877–2885, 1988.

[20] Z. Wu, W. Happer, and J. M. Daniels, "Coherent nuclear-spin interactions of adsorbed ^{131}Xe gas with surfaces", *Phys. Rev. Lett.*, vol. 59, no. 13, pp. 1480–1483, 1987.

[21] Z. Wu, S. Schaefer, G. D. Cates, and W. Happer, "Coherent interactions of the polarized nuclear spins of gaseous atoms with the container walls", *Phys. Rev. A*, vol. 37, no. 4, pp. 1161–1175, 1988.

1558-1748 (c) 2019 IEEE. Personal use is permitted, but republication/redistribution requires IEEE permission. See http://www.ieee.org/publications_standards/publications/rights/index.html for more information.